A model-based control design approach for linear free-piston engines

Article (Accepted Version)

A MODEL-BASED CONTROL DESIGN APPROACH FOR LINEAR FREE-PISTON ENGINES

T. N. Kigezi
Department of Engineering and Design
The School of Engineering and Informatics
The University of Sussex, Falmer, Brighton, BN1 9QT, UK.
T.Nsabwa-Kigezi@sussex.ac.uk

J. F. Dunne[1]
Department of Engineering and Design
The School of Engineering and Informatics
The University of Sussex, Falmer, Brighton, BN1 9QT, UK.
j.f.dunne@sussex.ac.uk

[1]Corresponding author

Summary

A general design approach is presented for model-based control of piston position in a free-piston engine (FPE). The proposed approach controls either 'bottom-dead-centre' (BDC) or 'top-dead-centre' (TDC) position. The key advantage of the approach is that it facilitates controller parameter selection, by way of deriving parameter combinations that yield both stable BDC and stable TDC. Driving the piston motion towards a target compression ratio is therefore achieved with sound engineering insight, consequently allowing repeatable engine cycles for steady power output. The adopted control design approach is based on linear control-oriented models derived from exploitation of energy conservation principles in a two-stroke engine cycle. Two controllers are developed: A Proportional Integral (PI) controller with an associated stability condition expressed in terms of controller parameters, and a Linear Quadratic Regulator (LQR) to demonstrate a framework for advanced control design where needed. A detailed analysis is undertaken on two FPE case studies differing only by rebound device type, reporting simulation results for both PI and LQR control. The applicability of the proposed methodology to other common FPE configurations is examined to demonstrate its generality.

26 main-section pages (double spaced) 27 references Figures 1 – 10 No Appendices

1. INTRODUCTION

Free-Piston engines (FPEs) are combustion-driven generators with controlled piston motion that has none of the kinematic restrictions imposed by a slider-crank mechanism. In contrast, piston motion in a conventional internal combustion (IC) engine is constrained by the fixed stroke of a slider-crank mechanism. Free of such constraints, FPEs allow variable stroke and compression ratio. Moreover, the absence of a crank mechanism means fewer moving parts, with lower friction losses, and greater compactness. The output of an FPE is realized by converting the piston force energy directly into electrical or hydraulic power. At present, electric power generation is the most common application of FPEs targeted for deployment as Auxiliary Power Units (APUs) in hybrid electric vehicles [1].

Because piston motion in an FPE is governed entirely by dynamic force interaction, active piston motion control is needed for stable and repeatable engine cycles. As the piston dead-centre positions (i.e. BDC or TDC) are free to vary cycle-by-cycle, accurate piston control is not only essential to ensure sufficient scavenging and compression ratio for combustion, but also ensures sufficient clearance to avoid the piston colliding with the cylinder-head. The central problem then is control of compression ratio i.e. control of TDC or BDC position. Secondly, controlling the piston to follow a given trajectory has been tested in starting the engine [2,3], and in achieving robustness against misfire [4,5]. Additionally, cycle frequency manipulation is viable in some applications and has been tested [6,7].

Although a number of prototype FPEs have been developed [8 - 10], no studies have adopted a fully analytical model-based approach to piston motion control in a general way so as to include various FPE configurations and types. Previous control approaches have largely considered the engine as a ‘black box’ - the shortcoming being, no real justification for the strategic basis adopted, and no corresponding stability assessment.

In TDC and BDC control, usually two separate control loops are involved. One control loop achieves BDC control by regulating the fuel supply, whereas the second achieves TDC control by regulating the energy stored in the rebound device, consequently regulating the rebound 'stiffness'. Tikkanen and Vilenius [11] are early proponents of a similar approach, highlighting the difficulty of achieving reliable piston motion control in practice. They proposed analytically-guided control of TDC and BDC using total energy flows to control compression ratio via a combination of fuel and piston load regulation – a potentially useful approach, although is left untested. By contrast, Johansen et al [12,13] derive a detailed dynamic model of a diesel FPE. Their control-oriented analysis reveals that TDC control can be achieved by varying rebound stiffness whereas BDC control can be achieved by regulation of injected fuel per cycle. They implement Proportional Integral (PI) and Proportional Integral Derivative (PID) controllers. Similarly, Mikalsen and Roskilly [14,15] implement separate TDC and BDC control strategies in their simulations of both spark ignition (SI) and compression ignition (CI) FPEs. They propose TDC control by regulating rebound stiffness per cycle, and BDC control by fuel regulation. Mikalsen and Roskilly [16] also identify the main difficulty of FPE control as being able to achieve sufficient compression ratio across what they call the 'entire load range'. This difficulty is further addressed in [17], with PID and other approaches examined in [18].

This paper sets out to develop and achieve a general, model-based, analytical approach to BDC and TDC control of a two-stroke FPE. In direct contrast to this work are non-model-based attempts to control BDC and TDC, where engineering insight into the control problem is achieved through trial and error – a potentially problematic approach, prone to unanticipated engine responses. The proposed model-based approach has two important benefits:

(i) In controller parameter selection: A range of viable parameters to warrant stable BDC and TDC can be computed prior to controller testing on hardware.

(ii) In availing a basis for advanced control design: A framework for advanced control

design is established, with the possibility of enforcing more stringent objectives other than stability; for example, requirements on optimality, robustness or constraint enforcement.

In the analysis presented here, energy conservation is exploited to derive control-oriented BDC and TDC dynamic models. These models are subsequently used to obtain a formal FPE stability condition in terms of the parameters of the widely-adopted PI controller. Furthermore, it is demonstrated how the models can be used to develop advanced control strategies such as Linear Quadratic Regulation (LQR) for optimality. This paper involves detailed extensions to the work of Gong et al [19], where model-based control for TDC is developed for a specific FPE configuration. A further step is taken in this paper to unify the approach into four common FPE configuration cases.

The paper is structured as follows: Section 2 describes FPE modelling, Section 3 describes control design and Section 4 considers four separate FPE configuration cases, generating numerical results by simulation.

2. FREE PISTON ENGINE DYNAMIC MODELLING

This section broadly introduces two kinds of FPE model. First, a general piston dynamics and gas thermodynamics model which captures fuel input and output power production – this will be used for simulating the FPE. Second, BDC and TDC energy-based control-oriented models are developed. These control-oriented models are used in BDC/TDC control design that follows in Section 3. The scope of the modelling is now summarized by stating the following assumptions:

(i) Zero-dimensional thermodynamic models are used to describe thermodynamic events in the FPE. Whereas sufficient to demonstrate this paper's BDC and TDC controller effectiveness, these models are of limited scope to describe performance aspects such

as fuel efficiency or emissions formation.

(ii) All fuel available is assumed to be completely combusted, with negligible effects from air-fuel ratio variability. Indeed, air-fuel ratio is regarded as a static parameter.

(iii) Ideal scavenging occurs, where all exhaust gas is completely expunged and instantaneously replaced with fresh charge. Therefore, the effect of residual gases or exhaust gas recirculation to combustion chamber thermodynamics is not considered.

(iv) As the focus is on achieving stable BDC and TDC control on the engine side, investigation into the electrical energy conversion efficiency (and its variability with BDC and TDC) on the generator side is deemed out of scope of this work.

The scope boundaries (i) - (iii) are not unusual in IC engine analysis for control design [20].

2.1 General Dynamic Engine Model

An idealised two-stroke FPE design concept is shown in Figure 1 comprising a single piston, a translator rod, a permanent magnet generator, and a rebound device (which could either be a mechanical spring or an air bounce chamber). Starting at BDC position x_b, the piston is pushed by the rebound device on the compression stroke to TDC position x_t. Combustion takes place in the trapped volume between x_t and the cylinder head, driving the piston back to position x_b during the expansion stroke at the which scavenging occurs. Under ideal conditions, this cycle repeats itself but in general x_b and x_t are free to vary from cycle-to-cycle to yield a variable compression ratio. The electrical machine converts the piston rod thrust energy directly into a useful output electrical power. In general, the output could also be hydraulic power.

To construct the equations of motion for a free piston engine, Newtonian mechanics and combustion thermodynamics are used. Taking the compression stroke as the positive direction, Newton's 2nd law gives:

$$-m_p \ddot{x} = F_G + F_L + F_{RD} \tag{1}$$

where m_p is the piston-translator mass, and the forces on the right-hand-side are obtained as follows: the in-cylinder gas force is given by $F_G = A_p P_G$, where P_G is the in-cylinder gas pressure which, other than at scavenging, can be obtained from the single-zone thermodynamics model [21] as:

$$\frac{dP_G}{dt} + \frac{\gamma}{V_G}\frac{dV_G}{dt}P_G = \frac{\gamma - 1}{V_G}\left(\frac{dQ_{ch}}{dt} - \frac{dQ_{ht}}{dt}\right) \tag{2}$$

where Q_{ch} is the gross heat release from fuel ignition, Q_{ht} is the heat transfer out of the combustion chamber, V_G is instantaneous cylinder volume, and γ is a heat capacity ratio of the working gas. The gross heat release rate is given by:

$$\frac{dQ_{ch}}{dt} = \eta_c Q_{LHV} u_G \frac{dx_\beta}{dt} \tag{3}$$

where Q_{LHV} is the fuel lower heating value, u_G is the fuel mass, x_β is the fuel mass-fraction-burned given by a time-based Wiebe function, and η_c is the combustion efficiency (usually 95%-98% [21]), known to vary at least with air-fuel ratio [20]. The heat transfer rate is given by:

$$\frac{dQ_{ht}}{dt} = hA_s\left(T - T_w\right) \tag{4}$$

where T_w is the cylinder wall temperature, T is the gas temperature computed from the ideal gas equation relating temperature, volume and pressure (from equation (2)), A_s is the surface area enclosing the combustion volume, and h is a heat transfer coefficient, for example given by Hohenberg [22]. The FPE electrical power generation arises from a piston load force F_L assumed proportional to piston velocity i.e.

$$F_L = \mu\dot{x} \tag{5}$$

where μ is an electrical machine constant typically called the generator coefficient. The rebound device force depends on whether it is a spring or an air bounce chamber:

$$F_{RD} = \begin{cases} k_s x, & \text{mechanical spring} \\ -A_p P_{RD}, & \text{bounce chamber} \end{cases} \tag{6}$$

where k_s is the spring stiffness, and P_{RD} corresponds to the bounce chamber pressure that in general satisfies a polytropic process law: $P_{RD} V_{RD}^{\gamma} = \text{constant}$.

2.2 Control Oriented Engine Models

The general dynamic engine model above describes continuous behaviour of the piston throughout a cycle. However, the piston only arrives at BDC or TDC once every cycle. The control oriented models developed next, seek to capture this discrete cycle behaviour through exploitation of energy conservation.

2.2.1 A 'bottom dead centre' (BDC) control-oriented energy balance model

A BDC control-oriented energy balance model is developed starting with simplifying assumptions and definitions associated with the cycle of an FPE as follows:

i) A new cycle commences at the start of the compression stroke, at piston position x_b.
ii) The end of the compression stroke occurs at piston position x_t.
iii) The start of the expansion stroke occurs at piston position x_t.
iv) The end of the expansion stroke occurs at piston position x_{b^+}.

These simplifying assumptions and definitions (i) - (iv) allow two energy balance relations to be constructed. The first is a compression-stroke energy balance statement as follows:

$$\underset{b\to t}{W_{RD}} = \underset{b\to t}{W_G} + \underset{b\to t}{E} \tag{7}$$

where $\underset{b\to t}{W_{RD}}$ is work done by the rebound device in pushing the piston from x_b to x_t, $\underset{b\to t}{W_G}$ is work done on the gas contained in cylinder when piston moves from x_b to x_t, and $\underset{b\to t}{E}$ is the energy converted by piston motion associated with the useful output energy and friction, when the piston moves from x_b to x_t. The second energy balance relation is an expansion-stroke statement:

$$\underset{t\to b^+}{W_G} = \underset{t\to b^+}{W_{RD}} + \underset{t\to b^+}{E} \tag{8}$$

where $\underset{t\to b^+}{W_G}$ is the work done by the gas in the cylinder driving the piston from x_t to x_{b^+}, $\underset{t\to b^+}{W_{RD}}$ is the work done on the rebound device when the piston moves from x_t to x_{b^+}, and $\underset{t\to b^+}{E}$ is the energy converted by the piston motion associated with useful output energy and friction when the piston moves from x_t to x_{b^+}.

Addition of the energy balance equation (7) and equation (8), gives the full-cycle energy balance:

$$\left(\underset{b\to t}{W_{RD}} - \underset{t\to b^+}{W_{RD}}\right) + \left(\underset{t\to b^+}{W_G} - \underset{b\to t}{W_G}\right) - \left(\underset{b\to t}{E} + \underset{t\to b^+}{E}\right) = 0 \tag{9}$$

Equation (9) can be used to predict x_{b^+} when x_t and x_b are known. A visual description of the piston motion in one cycle is given in Figure 2 (it shows the motion from one trough to the next, as a solid line). Index $k = 1,2,3,...$ is used to denote the cycle count of the piston end points, where x_T and x_B are the nominal end points, u_G is the fuel added to the cylinder for a given cycle. The input variable u_{RD} varies per cycle to adjust the stiffness of the rebound device. In a bounce chamber for example, u_{RD} is the trapped air mass which when varied per cycle adjusts the bounce chamber's stiffness on a cycle-by-cycle basis. Variable u_{RD} has no relevance for a mechanical spring.

In general, assuming isentropic compression and expansion processes, the first two parenthesized terms of equation (9) can be expressed in terms of the piston endpoint variables $\left(x_{b_{k+1}}, x_{t_k}, x_{b_k}, x_{t_{k-1}}\right)$ and the input variables $\left(u_{G_k}, u_{RD_k}\right)$ - this generality is later demonstrated in the development of three numerical case studies in Section 4 using the same six variables. Furthermore, the last parenthesized term of equation (9) which represents the total energy

converted in a cycle, is assumed to be approximated by a polynomial function of the piston end points, where, for small load changes, the total energy converted is approximately constant. Equation (9) may alternatively be expressed as an implicit nonlinear function in the form:

$$f_1\left(x_{b_{k+1}}, x_{t_k}, x_{b_k}, x_{t_{k-1}}, u_{G_k}, u_{RD_k}\right) = 0 \tag{10}$$

By defining a nominal point for the variables of interest i.e.:

$$\underline{\theta} = (x_B, x_T, U_G, U_{RD}) \tag{11}$$

where U_G and U_{RD} respectively depict the cylinder and rebound device inputs required to send the piston from x_T to x_B and x_B to x_T, the associated error variables from nominal $\underline{\theta}$ are defined as:

$$\begin{aligned} \delta x_b &= x_b - x_B \\ \delta x_t &= x_t - x_T \\ \delta u_G &= u_G - U_G \\ \delta u_{RD} &= u_{RD} - U_{RD} \end{aligned} \tag{12}$$

Equation (10), when expanded in the form of a Taylor series about the point $\underline{\theta}$, can be used to generate the following predictive equation:

$$\delta x_{b_{k+1}} = a_1 \delta x_{b_k} + b_1 \delta u_{G_k} + \xi_{1_k} \tag{13}$$

where:

$$\xi_{1_k} = c_1 \delta x_{t_k} + d_1 \delta x_{t_{k-1}} + e_1 \delta u_{RD_k} + g_1, \tag{14}$$

$$\begin{aligned} a_1 &= -\frac{\partial f_1}{\partial x_{b_k}} \Bigg/ \left.\frac{\partial f_1}{\partial x_{b_{k+1}}}\right|_{\underline{\theta}}, b_1 = -\frac{\partial f_1}{\partial u_{G_k}} \Bigg/ \left.\frac{\partial f_1}{\partial x_{b_{k+1}}}\right|_{\underline{\theta}}, c_1 = -\frac{\partial f_1}{\partial x_{t_k}} \Bigg/ \left.\frac{\partial f_1}{\partial x_{b_{k+1}}}\right|_{\underline{\theta}}, \\ d_1 &= -\frac{\partial f_1}{\partial x_{t_{k-1}}} \Bigg/ \left.\frac{\partial f_1}{\partial x_{b_{k+1}}}\right|_{\underline{\theta}}, e_1 = -\frac{\partial f_1}{\partial u_{RD_k}} \Bigg/ \left.\frac{\partial f_1}{\partial x_{b_{k+1}}}\right|_{\underline{\theta}}, g_1 = -f_1 \Bigg/ \left.\frac{\partial f_1}{\partial x_{b_{k+1}}}\right|_{\underline{\theta}} \end{aligned} \tag{15a-f}$$

Equation (13) is the BDC control-oriented prediction model which describes the deviation from nominal as a discrete-time, first order, linear time invariant (LTI) equation with input δu_G, output

δx_b and known residual term ξ_1 from the Taylor series expansion procedure, evaluated according to equation (14).

2.2.2 A 'top dead centre' (TDC) control-oriented energy balance model

The development of a TDC control-oriented energy balance model is similar to the BDC control-oriented model but with different end points, namely:

i) A new cycle starts at the beginning of the expansion stroke at piston position x_t.
ii) The end of the expansion stroke occurs at piston position x_b.
iii) The start of the compression stroke occurs at piston position x_b.
iv) The end of the compression stroke occurs at piston position x_{t^+}.

The corresponding expansion and compression stroke energy balance equation, analogous to equation (9), is:

$$\left(W_{RD_{b\to t^+}} - W_{RD_{t\to b}}\right) + \left(W_{G_{t\to b}} - W_{G_{b\to t^+}}\right) - \left(E_{t\to b} + E_{b\to t^+}\right) = 0 \tag{16}$$

Equation (16) can be used to predict x_{t^+} when x_b and x_t are known. Visualization making use of Figure 3 helps to picture a full engine cycle (peak-to-peak on the solid line) and associated piston end points, where k is the count index. Assuming isentropic compression and expansion, the first two parenthesized terms of equation (16) can be directly expressed in terms of the piston endpoint variables $\left(x_{t_{k+1}}, x_{b_k}, x_{t_k}, x_{b_{k-1}}\right)$ as well as the input variables $\left(u_{RD_k}, u_{G_k}, u_{RD_{k-1}}\right)$.

The last parenthesized term in equation (16) can be expressed as a polynomial function of the piston endpoint variables, which is nearly constant for small load changes. Similarly, equation (16) may be equivalently expressed as an implicit function:

$$f_2\left(x_{t_{k+1}}, x_{b_k}, x_{t_k}, x_{b_{k-1}}, u_{RD_k}, u_{G_k}, u_{RD_{k-1}}\right) = 0 \tag{17}$$

which, when expanded as a Taylor series about $\underline{\theta}$ and rearranged, yields the predictive equation:

$$\delta x_{t_{k+1}} = a_2 \delta x_{t_k} + b_2 \delta u_{RD_k} + \xi_{2_k} \tag{18}$$

where:

$$\xi_{2_k} = c_2 \delta x_{b_k} + d_2 \delta x_{b_{k-1}} + e_2 \delta u_{G_k} + g_2 \delta u_{RD_{k-1}} + h_2, \tag{19}$$

and where:

$$a_2 = -\frac{\partial f_2}{\partial x_{t_k}} \Bigg/ \left.\frac{\partial f_2}{\partial x_{t_{k+1}}}\right|_{\underline{\theta}},\ b_2 = -\frac{\partial f_2}{\partial u_{RD_k}} \Bigg/ \left.\frac{\partial f_2}{\partial x_{t_{k+1}}}\right|_{\underline{\theta}},\ c_2 = -\frac{\partial f_2}{\partial x_{b_k}} \Bigg/ \left.\frac{\partial f_2}{\partial x_{t_{k+1}}}\right|_{\underline{\theta}},\ d_2 = -\frac{\partial f_2}{\partial x_{b_{k-1}}} \Bigg/ \left.\frac{\partial f_2}{\partial x_{t_{k+1}}}\right|_{\underline{\theta}},$$
$$e_2 = -\frac{\partial f_2}{\partial u_{G_k}} \Bigg/ \left.\frac{\partial f_2}{\partial x_{t_{k+1}}}\right|_{\underline{\theta}},\qquad g_2 = -\frac{\partial f_2}{\partial u_{RD_{k-1}}} \Bigg/ \left.\frac{\partial f_2}{\partial x_{t_{k+1}}}\right|_{\underline{\theta}},\qquad h_2 = -f_2 \Bigg/ \left.\frac{\partial f_2}{\partial x_{t_{k+1}}}\right|_{\underline{\theta}} \tag{20a-g}$$

Equation (18) is the TDC control-oriented energy balance model which describes deviation from nominal as a discrete time, first order, LTI equation with input δu_{RD}, output δx_t, and known residual term ξ_2 from the Taylor series expansion procedure, evaluated according to equation (19).

3. CONTROL DESIGN

With BDC and TDC models constructed, design of feedback control action is possible to satisfy specific control objectives. Equations (13) and (18) (when suffixes 1, 2, and t are omitted) are of the same general form:

$$\delta x_{k+1} = a \delta x_k + b \delta u_k + \xi_k \tag{21}$$

and can therefore be treated similarly in subsequent analysis. The control objective is to design control action δu to stabilize the output, i.e. to drive δx to zero as $k \to \infty$. But for convenience, equation (21) can be simplified further, and by so doing, allows simplification of the subsequent analysis. Consider an equivalent input v defined as:

$$v_k = b \delta u_k + \xi_k \tag{22}$$

which allows equation (21) to be rewritten as:

$$\delta x_{k+1} = a\delta x_k + v_k \tag{23}$$

The control objective now becomes the design of an equivalent input v that drives the output δx_{k+1} to zero as $k \to \infty$. Note that when the equivalent control v is designed for equation (23), it is ultimately implemented for equation (21) as:

$$\delta u_k = \frac{1}{b}\left(v_k - \xi_k\right) \tag{24}$$

as per the relation between v and δu in equation (22).

3.1 Proportional-Integral Control Design

Proportional-Integral (PI) control, which is well-suited to low order linear systems, has been shown to provide effective control in simulation and experimental work on FPEs [3 – 6]. Since equation (23) represents a first order linear system, PI control is appropriate for BDC and TDC control of FPEs. Moreover, an associated stability condition can be derived. The input-output transfer function for equation (23) is found as:

$$G(z) = \frac{z^{-1}}{1 - az^{-1}} \tag{25}$$

where z is the unit delay operator. For a reference value $r = 0$, the feedback error is defined as $e_k = r - \delta x_k$. Defining the integral of the feedback error as $I_k = e_{k-1} + I_{k-1}$, a PI controller is realised as:

$$v_k = k_p e_k + k_i I_k \tag{26}$$

where $k_p > 0$ and $k_i > 0$. The transfer function from equation (26) (i.e. the feedback error to control input) is given as:

$$C(z) = \frac{k_p + \left(k_i - k_p\right)z^{-1}}{1 - z^{-1}} \tag{27}$$

The plant model equation (25) and the controller (27) are in a closed negative-feedback loop, whose transfer function relates the reference input to the output, and has the well-known form:

$$G_{CL}(z) = \frac{CG}{1+CG} \tag{28}$$

with two poles p_1 and p_2 are evaluated as:

$$p_1 = \frac{-\beta + \sqrt{\beta^2 - 4\alpha\gamma}}{2\alpha},\ p_2 = \frac{-\beta - \sqrt{\beta^2 - 4\alpha\gamma}}{2\alpha} \tag{29}$$

where $\alpha = 1, \beta = (k_p - a - 1)$, and $\gamma = (k_i - k_p + a)$, in terms of the parameters k_p and k_i. For stability of this closed loop system, the poles p_1 and p_2 must lie within the unit circle to imply that the output δx decays to zero as time goes to infinity. Another way to express this statement is:

$$|p_1| \cdot |p_2| = |p_1 p_2| < 1 \tag{30}$$

which manifests a closed form stability condition for PI control in terms of parameters k_p and k_i. In simple terms, for a given value of k_p, the integral gain k_i must be chosen to satisfy (30). Indeed, a useful map showing regions of stable and unstable parameter combinations can easily be generated, as is shown in Figure 4.

3.2 Advanced Control Design

Requirements, other than stability and output decay to zero, can be imposed on the control action such as optimality, robustness, and even constraint enforcement. Here optimality of the control action (relating to minimization of a mathematically defined performance index) is considered i.e. achieving an optimal fuel supply or optimal regulation of the rebound device stiffness. Linear quadratic regulation via a state space control design formalism is pursued for illustrative purposes. For improved controller performance, integral action υ is applied to the output as:

$$\upsilon_{k+1} = \delta x_k + \upsilon_k \tag{31}$$

By constructing the state vector $\mathrm{w}=\left[\delta \mathrm{x} \quad \upsilon\right]^{\mathrm{T}}$, both equation (23) and (31) can then be directly expressed in state space form as:

$$\mathrm{w}_{\mathrm{k}+1}=\mathrm{A}\mathrm{w}_{\mathrm{k}}+\mathrm{B}\mathrm{v}_{\mathrm{k}} \tag{32}$$

where

$$\mathrm{A}=\begin{bmatrix}\mathrm{a} & 0\\ 1 & 1\end{bmatrix}, \mathrm{B}=\begin{bmatrix}1\\ 0\end{bmatrix} \tag{33a, b}$$

To ensure stability of (32), and decay of w to zero as $\mathrm{k}\to\infty$, the control law is:

$$\mathrm{v}_{\mathrm{k}}=-\mathrm{K}\mathrm{w}_{\mathrm{k}} \tag{34}$$

where the state feedback gain K is chosen to ensure that the eigenvalues of matrix $\mathrm{A}-\mathrm{BK}$ lie within the unit circle. However, the optimal gain K that minimizes the performance objective function:

$$\mathrm{J}=\sum_{\mathrm{k}=0}^{\infty}\left(\mathrm{w}_{\mathrm{k}}^{\mathrm{T}}\mathrm{Q}\mathrm{w}_{\mathrm{k}}+\mathrm{u}_{\mathrm{k}}^{\mathrm{T}}\mathrm{R}\mathrm{u}_{\mathrm{k}}\right) \tag{35}$$

is computed from:

$$\mathrm{K}=\left(\mathrm{B}^{\mathrm{T}}\mathrm{P}\mathrm{B}+\mathrm{R}\right)^{-1}\mathrm{B}^{\mathrm{T}}\mathrm{P}\mathrm{A} \tag{36}$$

where Q and R in equation (35) are appropriately chosen positive-definite weight matrices, and where P is a positive definite matrix that is a solution to the Riccati equation [23]:

$$\mathrm{Q}+\mathrm{A}^{\mathrm{T}}\mathrm{P}\mathrm{A}-\mathrm{P}-\mathrm{A}^{\mathrm{T}}\mathrm{P}\mathrm{B}\left(\mathrm{B}^{\mathrm{T}}\mathrm{P}\mathrm{B}+\mathrm{R}\right)^{-1}\mathrm{B}^{\mathrm{T}}\mathrm{P}\mathrm{A}=0 \tag{37}$$

4. CASE STUDIES - TESTING BY SIMULATION

The generic modelling and control design developed in the previous sections will now be tailored to specific FPE configuration cases – all physically dissimilar, but with conceptually identical configurations. Detailed development for each particular case will precede the test simulation results. Two cases of FPEs, differing only by rebound device type, namely the case

of a mechanical spring, and the case of a bounce chamber, are first studied. In these studies, Figures 2 and 3 shall be used for reference purposes. Examination will then follow for two other common FPE cases, with one involving two opposed pistons in the same cylinder.

Note that in all simulations, the cylinder pressure is modelled using the Single Zone thermodynamic model with a time-dependent Wiebe function for heat release adapted from [21]. Perfect scavenging is assumed, with the intake pressure taken as standard atmospheric pressure. The dynamic behavior of an FPE follows from [5, 8] where the electrical generator force is assumed to be proportional to piston speed - a typical assumption with free-piston engine generators (FPEGs). Table 1 gives the FPE geometric parameters used in simulations.

4.1 Case I: Mechanical Spring as Rebound Device

In this configuration, the FPE rebound device (label (5) in Figure 1) is simply a mechanical spring [24] [25]. As the spring stiffness is fixed, the only control variable available for BDC control is fuel supply. Whereas the objective of BDC control is to ensure the piston is driven to nominal BDC, it is possible to compute the spring stiffness needed to send the piston from nominal BDC to nominal TDC.

4.1.1 Detailed development of the control-oriented model for BDC control

The first task is to construct the specific form of equation (9). If the spring stiffness is denoted by k_s, the first parenthesized term in equation (9) becomes:

$$W_{\substack{RD\\ b\to t}} - W_{\substack{RD\\ t\to b^+}} = \left\{\frac{1}{2}k_s\left(x_{b_k}^2 - x_{t_k}^2\right)\right\} - \left\{-\frac{1}{2}k_s\left(x_{t_k}^2 - x_{b_{k+1}}^2\right)\right\} \tag{38}$$

which, as expected, is a function only of the piston endpoints. Pressure varies with volume in an isentropic process according to:

$$PV^{\gamma} = \begin{cases}\text{constant 1; compression stroke}\\ \text{constant 2; expansion stroke}\end{cases} \tag{39}$$

where γ is the heat capacity ratio of the working gas. Therefore, from the isentropic work done, the second parenthesized term is:

$$\underset{t\to b^+}{W_G}-\underset{b\to t}{W_G}=\left\{\frac{P_{G_{b^+}}V_{G_{b^+}}-\left(P_{G_t}+\Delta P_{G_t}\right)V_{G_t}}{1-\gamma}\right\}-\left\{-\frac{P_{G_t}V_{G_t}-P_{G_b}V_{G_b}}{1-\gamma}\right\} \tag{40}$$

where P_G is in general the in-cylinder gas pressure, ΔP_G is the pressure rise at constant volume, V_G is the cylinder volume, and P_{G_b} is the air intake pressure during scavenging (which must be known). Using equation (39) in equation (40):

$$\underset{t\to b^+}{W_G}-\underset{b\to t}{W_G}=\left\{\frac{\left(P_{G_t}+\Delta P_{G_t}\right)\left(V_{G_t}^{\gamma}V_{G_{b^+}}^{1-\gamma}-V_{G_t}\right)}{1-\gamma}\right\}-\left\{-\frac{P_{G_b}\left(V_{G_b}^{\gamma}V_{G_t}^{1-\gamma}-V_{G_b}\right)}{1-\gamma}\right\} \tag{41}$$

where the pressure P_{G_t} can be evaluated from equation (39) as:

$$P_{G_t}=P_{G_b}\left(\frac{V_{G_b}}{V_{G_t}}\right)^{\gamma} \tag{42}$$

Turning to the combustion pressure rise term ΔP_{G_t}, if the total amount of fuel burned at constant volume V_{G_t} is u_G, then the corresponding pressure rise is given by:

$$\Delta P_{G_t}=\frac{\eta_c Q_{LHV} R}{c_v}\left(\frac{1}{V_{G_t}}\right)u_{G_t} \tag{43}$$

where η_c is the combustion efficiency, u_{G_t} is the fuel mass input for a given cycle, Q_{LHV} is the fuel lower heating value, R is the specific gas constant, and c_v is the specific heat capacity of the gas at constant volume.

Thus, using equations (39), (42), and (43), equation (40) can be expressed as a function of cylinder volume and fuel input only. Since the cylinder volume depends on piston position (see example formulation in (47)), equation (40) therefore depends only on the piston end points

and the fuel mass input. The third term of equation (9) as stated earlier, can, under low load changes, be approximated as a constant i.e.:

$$\underset{b\to t}{E}+\underset{t\to b^{+}}{E}=\{E_1\}+\{E_2\} \tag{44}$$

where E_1 and E_2 are constants. The sum of equations (38), (40), and (44) combine to form a nonlinear equation of the form:

$$f_1\left(x_{b_{k+1}}, x_{t_k}, x_{b_k}, u_{G_k}\right)=0 \tag{45}$$

as shown by equation (10). A Taylor series expansion of equation (45) will generate the particular form of the BDC control-oriented model for equation (13) – the subsequent controller follows directly from the steps described in equations (21) – (37).

4.1.2 Assignment of the spring stiffness

The energy required by the piston to move from nominal BDC to nominal TDC during the compression stroke is supplied entirely by the rebound device – in this case, a mechanical spring. An appropriate choice of the spring stiffness ensures that the piston moving from nominal BDC precisely reaches nominal TDC. This is achieved using the compression stroke energy balance equation (7) evaluated at nominal piston end points. The spring stiffness obtained is:

$$k_s=\frac{2P_{G_b}V_{G_b}^{\gamma}V_{G_t}^{1-\gamma}\left(1-r_c^{\,1-\gamma}\right)+2(\gamma-1)E_1}{(\gamma-1)\left(x_B^2-x_T^2\right)} \tag{46}$$

where $r_c=V_{G_b}/V_{G_t}$ is the nominal compression ratio, x_B and x_T are the nominal BDC and nominal TDC piston displacement positions respectively.

4.1.3 TDC Estimation

Implementation of the control action in equation (24) for BDC control requires BDC feedback (as δx_{b_k} in v_k) and feedback of the immediately-following TDC position (as δx_{t_k} in ξ_k). Whereas

the BDC feedback can be made available by a sensor, the immediately-following TDC position must be estimated when the piston is at the BDC position. This can be done as follows: in Figure 1, let l be the length from the left end of the cylinder to centre line $x = 0$. Considering the direction to the left of centre line $x = 0$ as positive, and to the right of centre line as negative, then the instantaneous in-cylinder volume for a piston crown of area A_p is given as:

$$V_G = A_p (l - x) \tag{47}$$

Hence using equation (47), a TDC estimate is given as:

$$\hat{x}_t = l - \frac{\hat{V}_{G_t}}{A_p} \tag{48}$$

where $\hat{V}_{G_t}$ is an estimate of the cylinder volume at the estimated TDC position $\hat{x}_t$.

Using the compression stroke energy balance equation (7) and equation (48), an algebraic equation can be constructed for $\hat{V}_{G_t}$ as follows:

$$p\hat{V}_{G_t}^2 + q\hat{V}_{G_t} + r\hat{V}_{G_t}^{1-\gamma} + s = 0 \tag{49}$$

where the coefficients are:

$$\begin{aligned} p &= \frac{1}{2A_p^2} k_s (1-\gamma) \\ q &= -\frac{1}{A_p} k_s l (1-\gamma) \\ r &= -P_{G_b} V_{G_b}^{\gamma} \\ s &= P_{G_b} V_{G_b}^{\gamma} + (1-\gamma)\left\{ E_1 + E_2 + \frac{1}{2} k_s (l^2 - x_b^{\,2}) \right\} \end{aligned} \tag{50a-d}$$

Equation (49) can be solved numerically, for example via Newton's method, and used in equation (48) to compute the TDC estimate. The iterations can be expected to converge quickly given that an initial solution guess (for example nominal TDC) is not far from the true TDC

solution in a transient. In the simulation results, the number of iterations to find a solution was never greater than 5.

To make the spring constant computation via equation (46) exact, the electrical generator can be turned-off during the compression stroke, therefore rendering E_1 equal to zero. The nominal piston endpoints x_B and x_T are known, or easily calculated from the required compression ratio. The nominal inputs u_G and u_{RD} must be estimated – and the more accurate the estimates, the better the controller performance.

4.1.4 Simulation Results and Discussion

Testing the control of BDC and TDC for the case of a mechanical spring as a rebound device can now proceed. The FPE geometry is taken from Table 1, with the PI controller parameters k_p and k_i selected from the stability map in Figure 4, and the LQR weighting parameters Q and R selected as positive definite. It should be emphasized that only model-based control, such as developed, allows the confident selection of the controller parameters i.e. from a pre-determined set. The alternative is non-model-based control, which relies on a trial and error approach to obtain meaningful engineering insight.

Figure 5 shows the piston error at BDC and TDC for both PI and LQR control, having started with an offset and going to zero after a relatively small number of cycles. Hence a steady compression ratio is achieved. The piston error at BDC and TDC is expressed as the percentage:

$$\frac{\text{Deviation from nominal BDC/TDC}}{\text{Nominal BDC/TDC}} \times 100 \tag{51}$$

which must stay below a critical value (which for the geometry considered is 24%, indicating where the deviation corresponds to the cylinder clearance length). In this case, the LQR control transient is slower than the PI control transient, owing to a minimization of an objective function

that involves the fuel input (see equation (35)). Correspondingly the 'Supplied fuel input' in Figure 5, shows that the LQR transient fuel supply is lower than that with PI control. However, the FPE being an energy balance system at oscillations of constant amplitude (i.e. constant compression ratio), the fuel supplied at steady state is the same amount required to overcome a given load, regardless of the controller implemented. Therefore, the choice of one controller over another should be made based on transient response performance.

The performance responses of the electrical power produced (deduced from equation (5)), and piston oscillation frequency (or engine speed), are shown in Figure 6. As expected, when steady compression ratio is achieved, both show stable convergence to the same value at steady state. In the simulation, an initial piston position is chosen such that the initial BDC/TDC error is small but significant (around 5%). In practice, a starting arrangement is required to bring the piston from its rest position as close to nominal BDC/TDC as possible before engine firing. This ensures that nominal compression ratio is achieved first. The largest possible initial BDC/TDC error that yields a compression ratio sufficient for combustion can be investigated experimentally.

4.2 Case II: Bounce Chamber as Rebound Device

In this configuration, the rebound device is a stiffness adjustable air bounce chamber (or gas spring) [5, 6, 11, 12]. The chamber usually changes the air mass once every cycle to achieve TDC control. By varying the air mass, the bounce chamber stiffness is varied.

4.2.1 Detailed development of the control-oriented model for BDC control

As in the previous example, the first task is to construct the BDC control model via equation (9). Considering isentropic expansion and compression of the rebound device, this specializes to:

$$W_{\substack{RD \\ b\to t}} - W_{\substack{RD \\ t\to b^+}} = \left\{ \frac{P_{RD_b}\left(V_{RD_b}^{\gamma} V_{RD_t}^{1-\gamma} - V_{RD_b}\right)}{1-\gamma} \right\} - \left\{ - \frac{P_{RD_b}\left(V_{RD_b}^{\gamma} V_{RD_{b^+}}^{1-\gamma} - V_{RD_b}^{\gamma} V_{RD_t}^{1-\gamma}\right)}{1-\gamma} \right\} \tag{52}$$

Assuming an ideal gas, and denoting the mass of air in the bounce chamber as u_{RD}, the pressure term P_{RD_b} in equation (52) is evaluated according to the ideal gas law as:

$$P_{RD_b} = RT_{RD_b}\left(\frac{1}{V_{RD_b}}\right)u_{RD_b} \tag{53}$$

where R is the specific gas constant, and T_{RD_b} is the air temperature at BDC (assumed to be a known constant). The second parenthesized term of equation (9) remains as evaluated in equations (41) – (43) because the cylinder side is no different from the previous example. Also, the same approximation equation (44) holds. Thus, equation (9) is again expressed in general nonlinear form:

$$f_1\left(x_{b_{k+1}}, x_{t_k}, x_{b_k}, x_{t_{k-1}}, u_{G_k}, u_{RD_k}\right) = 0 \tag{54}$$

Subsequent linearization by Taylor series expansion to achieve the BDC control-oriented model equation (13), and subsequent control design is as described in equations (21) – (37).

4.2.2 Detailed development of the control-oriented model for TDC control

For the TDC model, the first parenthesized term of equation (16) can be adapted to the form:

$$W_{\substack{RD \\ b\to t^+}} - W_{\substack{RD \\ t\to b}} = \left\{ \frac{P_{RD_b}\left(V_{RD_b}^{\gamma} V_{RD_{t^+}}^{1-\gamma} - V_{RD_b}\right)}{1-\gamma} \right\} - \left\{ - \frac{P_{RD_t}\left(V_{RD_t}^{\gamma} V_{RD_b}^{1-\gamma} - V_{RD_t}\right)}{1-\gamma} \right\} \tag{55}$$

where the pressure term P_{RD_b} is computed as in equation (53). The pressure P_{RD_t} is obtained from:

$$P_{RD_t} = P_{RD_{b^-}}\left(\frac{V_{RD_{b^-}}}{V_{RD_t}}\right)^{\gamma} \tag{56}$$

and where, according to the ideal gas law:

$$P_{RD_{b^-}} = RT_{RD_{b^-}} \left(\frac{1}{V_{RD_{b^-}}} \right) u_{RD_{b^-}} \tag{57}$$

Using the same argument as in the previous example, the second parenthesized term of equation (16) is:

$$W_{\substack{G \\ t \to b}} - W_{\substack{G \\ b \to t^+}} = \left\{ \frac{\left(P_{G_t} + \Delta P_{G_t}\right)\left(V_{G_t}^{\gamma} V_{G_b}^{1-\gamma} - V_{G_t}\right)}{1-\gamma} \right\} - \left\{ - \frac{P_{G_b}\left(V_{G_b}^{\gamma} V_{G_{t^+}}^{1-\gamma} - V_{G_b}\right)}{1-\gamma} \right\} \tag{58}$$

And similar to equation (42), the following condition holds:

$$P_{G_t} = P_{G_b} \left(\frac{V_{G_{b^-}}}{V_{G_t}} \right)^{\gamma} \tag{59}$$

where P_{G_b} is the air intake pressure during scavenging, and the pressure rise ΔP_{G_t} is as stated in equation (43). The third parenthesized term of (16) is the same as that of equation (9) and is therefore evaluated no differently from equation (44). Equation (16) can thus be stated in the general nonlinear form:

$$f_2\left(x_{t_{k+1}}, x_{b_k}, x_{t_k}, x_{b_{k-1}}, u_{RD_k}, u_{G_k}, u_{RD_{k-1}}\right) = 0 \tag{60}$$

Taylor series expansion of equation (60) yields the control-oriented model corresponding to equation (13) - subsequent controller design follows the process described by equations (21) – (37).

4.2.3 TDC Estimation

Estimation of TDC is important in the implementation of the BDC controller. As in the previous Case, the compression stroke energy balance is used to obtain:

$$P_{RD_b} V_{RD_b}^{\gamma} \left(\hat{V}_{RD_t}^{1-\gamma} - V_{RD_b}^{1-\gamma} \right) + P_{G_b} V_{G_b}^{\gamma} \left(\hat{V}_{G_t}^{1-\gamma} - V_{G_b}^{1-\gamma} \right) - E_1 (1-\gamma) = 0 \tag{61}$$

where $\hat{V}_{RD_t}$ and $\hat{V}_{G_t}$ are estimates of the rebound device volume and the cylinder volume at the immediately-following TDC position respectively. Volumes $\hat{V}_{RD_t}$ and $\hat{V}_{G_t}$ are known functions of $\hat{x}_t$, thus when substituted in equation (61), $\hat{x}_t$ can be found as a direct solution.

4.2.4 Simulation Results and Discussion

The basic engine geometry for the numerical simulation is again given in Table 1, with the PI controller parameters k_p and k_i selected from the stability map in Figure 4 and the LQR weighting parameters Q and R selected as positive definite.

Figure 7 shows the piston response for PI and LQR control, plus the fuel supply input for both controllers. Both TDC and BDC errors can be seen to converge to zero (implying convergence to a steady compression ratio). Owing to minimization of the supplied input fuel in equation (35), the LQR response transient is evidently slower than the PI response. But the LQR response transient appears to be 'smoother', and on this basis, is preferable to the PI transient for the parameters chosen. Note that at steady state, the same fuel is supplied regardless of the type of controller.

The generated electrical power and the engine speed are shown in Figure 8, both converging to their respective steady-state values when a steady compression ratio is achieved. There is a brief initial deviation from a converging path for both transients. This can be attributed to the interaction of the BDC and TDC controllers, as well as possibly unmodelled dynamics in control design – for example, instantaneous fuel combustion is assumed during control design (see equation (43)), whereas the engine is simulated with finite-time fuel combustion (see equation (3)).

4.3 Case III: Combustion Chamber as Rebound Device

In this configuration (also known as a dual-piston FPE) the rebound device is a combustion chamber [26-27] identical to the left-hand cylinder in Figure 1. The engine therefore comprises

two pistons on either end (hence the 'dual-piston' reference) which produces two power strokes in a cycle – one in gas compression, and the other in gas expansion. The treatment of this case reduces to analyzing two identical combustion chambers, but considering one as a rebound device. Since a combustion chamber has already been accounted for in the previous two cases, this third Case does not present any particular new challenge. The first parenthesized term of equation (9) is found as:

$$W_{\substack{RD \\ b\to t}} - W_{\substack{RD \\ t\to b^+}} = \left\{ \frac{\left(P_{RD_b} + \Delta P_{RD_b}\right)\left(V_{RD_b}^{\gamma} V_{RD_t}^{1-\gamma} - V_{RD_b}\right)}{1-\gamma} \right\} - \left\{ - \frac{P_{RD_t}\left(V_{RD_t}^{\gamma} V_{RD_{b^+}}^{1-\gamma} - V_{RD_t}\right)}{1-\gamma} \right\} \tag{62}$$

where P_{RD_t} is the rebound device intake pressure during scavenging. Following the arguments used to obtain equations (42) and (43), P_{RD_b} and ΔP_{RD_b} are functions of: i) the rebound device cylinder volume (which itself is expressible as a function of piston endpoints), and ii) the rebound device fuel input u_{RD}. Since the left-hand cylinder remains unchanged following-on from the previous case, the second parenthesized term of equation (9) is evaluated in the same way as in equation (41) – (43). Also, the same approximation equation (44) holds. This allows equation (9) to be expressed in the general nonlinear form:

$$f_1\left(x_{b_{k+1}}, x_{t_k}, x_{b_k}, x_{t_{k-1}}, u_{G_k}, u_{RD_k}\right) = 0 \tag{63}$$

By Taylor series expansion, the control-oriented model equation (18) and subsequent controller design, again follow from the procedure described in equations (21) – (37). By swapping the cylinder functions on either end, the TDC control-oriented model is realized through the same process as the BDC control-oriented model.

Figure 9 shows the BDC and TDC error responses using the same simulation settings as described in the previous cases. As expected both errors converge to zero to yield a steady compression ratio at steady state. The LQR response transient is slower – owing to a fuel

minimization requirement in (35) – but also less oscillatory than the PI controller response, for the controller parameters used.

4.4 Case IV: Opposed Piston FPE

In this configuration, two opposing pistons share a combustion chamber to form an opposed piston FPE [10] as shown in Figure 10. It is shown here that under symmetry conditions, analysis of this configuration case for BDC and TDC control is no different from that for the previously studied cases. Symmetry about the centre line simplifies analysis of the device, by reducing the device to an equivalent single piston FPE configuration. This is achieved after noting that on Figure 10, the common combustion volume is given by:

$$V_G = V_{G_y} + V_{G_x} \tag{64}$$

where V_{G_y} and V_{G_x} are instantaneous gas chamber volumes on either side of the centre line. Assuming symmetry of piston motion, and identical physical properties on either side of the centre line, the two gas volumes are then equal i.e. $V_{G_y} = V_{G_x}$ giving:

$$V_G = 2V_{G_y} = 2V_{G_x} \tag{65}$$

From equation (65), the common volume is equivalently-described either by the left or right gas chamber volume. The common volume V_G is the only form of coupling between the two pistons, therefore symmetry acts as a decoupling condition. It can therefore be concluded from equation (65) that opposed piston FPE analysis under symmetry conditions is equivalent to single piston FPE analysis, but with twice the volume to the centre line. If the symmetry assumption does not hold, then this amounts to quantifying the asymmetry between the two opposing piston FPE. Knowledge of this asymmetry can then be compensated for in the equivalent single piston model. Thus, under asymmetry conditions, by defining the volume as:

$$V_{G_y} = V_{G_x} + \psi(t) \tag{66}$$

where $\psi(t)$ is the instantaneous time-varying volume difference between the left and right cylinder volumes to the centre line, for which $\psi(t)=0$ implies complete symmetry. Substituting equation (66) into equation (64) yields

$$V_G = 2V_{G_x} + \psi(t) \tag{67}$$

or, in terms of the left cylinder:

$$V_G = 2V_{G_y} - \psi(t) \tag{68}$$

Equations (67) and (68) are generalized forms of equation (65), taking into account asymmetry of the left and right cylinders as quantified by parameter $\psi(t)$. The common volume V_G is described only in terms of the left or right cylinder volume to the centre line. The general finding is that analysis of an opposed piston FPE configuration is equivalent to the analysis of just one piston, for example in Cases I, II and III, assuming the level of asymmetry between the two pistons is known, and adequately compensated for. It can be investigated whether the asymmetry parameter $\psi(t)$ can be modelled with simple and convenient functions that can be fitted to experimental data. This serves as a possible future line of investigation.

5. CONCLUSIONS

A model-based procedure for control of BDC and TDC in a free-piston engine has been developed, thereby achieving analytically-guided compression ratio control. The limited scope of zero-dimensional thermodynamic modelling does not permit a first-principled investigation into performance aspects such as fuel efficiency or emissions formation. However, the basic objective of analytically deriving controller parameter combinations that produce stable BDC/TDC responses has been achieved and demonstrated with PI control. Additionally, using LQR control, advanced control yielding transient responses that satisfy stated performance

objectives has been demonstrated. Of greater significance however is the unified context in which four FPE configurations can be treated to demonstrate the generality of the proposed approach.

References

[1] M. R. Hanipah, R. Mikalsen and A. Roskilly, "Recent commercial free piston engine developments for automotive applications," Applied Thermal Engineering, vol. 75, pp. 493-503, 2015.

[2] K. Li, A. Sadighi and Z. Sun, "Active Motion Control of a Hydraulic Free Piston Engine," IEEE/ASME Transactions on Mechatronics, vol. 19, no. 4, pp. 1148-1159, 2014.

[3] K. Li, C. Zhang and Z. Sun, "Precise piston trajectory control for a free piston engine," Control Engineering Practice, vol. 34, pp. 30-38, 2015.

[4] H. Kosaka, T. Akita, K. Moriya, S. Goto, Y. Hotta, T. Umeno and K. Nakakita, "Development of Free Piston Engine Linear Generator System Part 1 - Investigation of Fundamental Characteristics," SAE Technical Paper 2014-01-1203, 2014.

[5] S. Goto, K. Moriya, H. Kosaka, T. Akita, Y. Hotta, T. Umeno and K. Nakakita, "Development of Free Piston Engine Linear Generator System Part 2 - Investigation of Control System for Generator," SAE Technical Paper 2014-01-1193, 2014.

[6] P. A. J. Achten, J. P. J. Van den Oever, J. Potma and G. Vael, "Horsepower with brains: The design of the Chiron free piston engine," SAE Paper 2000–01–2545, 2000.

[7] A. Hbi and T. Ito, "Fundamental test results of a hydraulic free piston internal combustion engine," Proceedings of Institute of Mechanical Engineering, no. 218, pp. 1149–1157, 2004.

[8] R. Mikalsen and A. Roskilly, "A review of free-piston engine history and applications," Applied Thermal Engineering, no. 27, pp. 2339-2352, 2007.

[9] C. Toth-Nagy and N. N. Clark, "The Linear Engine in 2004," SAE Technical Paper 2005-01-2140, 2005.

[10] P. A. J. Achten, "A review of free piston engine concepts," SAE Paper 941776, 1994.

[11] S. Tikkanen and M. Vilenius, "Hydraulic Free Piston Engine – Challenge for Control," Proceedings of the 1999 European Control Conference, pp. 2943-2948, 1999.

[12] T. A. Johansen, O. Egeland, E. A. Johannessen and R. Kvamsdal, "Free-Piston Diesel Engine Dynamics and Control," Proceedings of the American Control Conference, pp. 4579-4584, 2001.

[13] T. A. Johansen, O. Egeland, E. A. Johannessen and R. Kvamsdal, "Free-Piston Diesel Engine Timing and Control—Toward Electronic Cam- and Crankshaft," IEEE Transactions on Control Systems Technology, vol. 10, no. 2, pp. 177-190, 2002.

[14] R. Mikalsen and A. P. Roskilly, "The design and simulation of a two-stroke free-piston compression ignition engine for electrical power generation," Applied Thermal Engineering, no. 28, pp. 589-600, 2008.

[15] R. Mikalsen and A. Roskilly, "Performance simulation of a spark ignited free-piston engine generator," Applied Thermal Engineering , no. 28, pp. 1726-33, 2008.

[16] R. Mikalsen and A. P. Roskilly, "The control of a free-piston engine generator. Part 1: Fundamental analyses," Applied Energy, vol. 87, pp. 1273-1280, 2009.

[17] R. Mikalsen and A. P. Roskilly, "The control of a free-piston engine generator. Part 2: Engine dynamics and piston motion control," Applied Energy, vol. 87, pp. 1281–1287, 2010.

[18] B. Jia, R. Mikalsen, A. Smallbone, Z. Zuo and H. Feng, "Piston motion control of a free-piston engine generator: A new approach," Applied Energy, vol. 179, pp. 1166–1175, 2016.

[19] X. Gong, K. Zaseck, I. Kolmanovsky and H. Chen, "Modeling and Predictive Control of Free Piston Engine Generator," Proceedings of the 2015 American Control Conference, pp. 4735-4740, 2015.

[20] L. Eriksson and L. Nielsen, Modeling and Control of Engines and Drivelines, John Wiley & Sons, 2014.

[21] J. B. Heywood, Internal Combustion Engine Fundamentals, McGraw-Hill, Inc., 1988.

[22] G. Hohenberg, "Advanced Approaches for Heat Transfer Calculations," SAE Paper 790825, 1979.

[23] B. D. O. Anderson and J. B. Moore, Optimal Control, Linear Quadratic Methods, Englewood Cliffs, New Jersey: Prentice-Hall, Inc., 1989.

[24] J. F. Dunne, "Dynamic Modelling and Control of Semifree-Piston Motion in a Rotary Diesel Generator Concept," Journal of Dynamic Systems, Measurement, and Control, vol. 132, no. 5, pp. 051003/1-051003/12, 2010.

[25] V. Gopalakrishnan, P. M. P Najt and R. P. Durrett, "US Patent: Free Piston Linear Alternator Utilizing Opposed Pistons with Spring Return," 2014.

[26] B. Jia, Z. Zuo, G. Tian, H. Feng and A. P. Roskilly, "Development and validation of a free-piston engine generator numeric model," Energy Conversion and Management, vol. 91, pp. 333-341, 2015.

[27] P. Van Blarigan, N. Paradiso and S. Goldsborough, "Homogeneous Charge Compression Ignition with a Free Piston: A New Approach to Ideal Otto Cycle Performance," SAE Technical Paper 982484, 1998.

Table Captions

Table 1. Parameter values for Free Piston Engine simulations

Figure Captions

Figure 1. Generic FPE schematic. The piston, translator, and generator permanent magnet (for this illustration of an FPE generator) constitute the moving mass. The rebound device may be a mechanical spring, an air bounce chamber or another cylinder.

Figure 2. Visualization of piston motion over time annotated with notation used in analysis. One complete cycle is from b to b^+. The lines x_T and x_B are the nominal piston endpoints. The arrows represent inputs to the engine as fuel addition or rebound device stiffness adjustment.

Figure 3. Visualization of piston motion over time annotated with notation used in analysis. One complete cycle is from t to t^+. The lines x_T and x_B are the nominal piston endpoints. The arrows represent inputs to the engine as fuel addition or rebound device stiffness adjustment.

Figure 4. Parameter combinations k_p, k_i and associated regions of stability or instability, where $a = 1.05$ in system (24).

Figure 5. BDC/TDC error and input fuel response for PI and LQR controllers with a mechanical spring as rebound device. Controller parameters were chosen within their stability bounds. LQR response transient is slower than the PI response transient owing to a minimization of input objective.

Figure 6. Output power and engine speed responses with a mechanical spring as rebound device. The same power and speed are achieved at steady state regardless of controller type.

Figure 7. BDC/TDC error and input fuel response for PI and LQR controllers with a bounce chamber as rebound device. Controller parameters were chosen within their stability bounds. LQR response transient is slower than the PI response transient owing to a minimization of input objective.

Figure 8. Output power and engine speed responses with a bounce chamber as rebound device. The same power and speed are achieved at steady state regardless of controller type.

Figure 9. BDC/TDC error response for PI and LQR controllers with a combustion chamber as rebound device. Controller parameters were chosen within their stability bounds. LQR response transient is slower than the PI response transient owing to a minimization of input objective.

Figure 10. An opposed piston FPE. Two pistons sharing a combustion volume oppose each other about the centre line.

List of Tables

Table 1. Parameter values for Free Piston Engine simulations

Parameter	Value
Nominal cylinder compression ratio	10.44
Nominal Cylinder displacement	0.5 litres
Bore	86 mm
Nominal Stroke	86 mm
Piston-translator mass	9.0 kg
Piston load (generator) coefficient	418.5 kg/s
Nominal compression ratio of bounce chamber	10

List of Figures

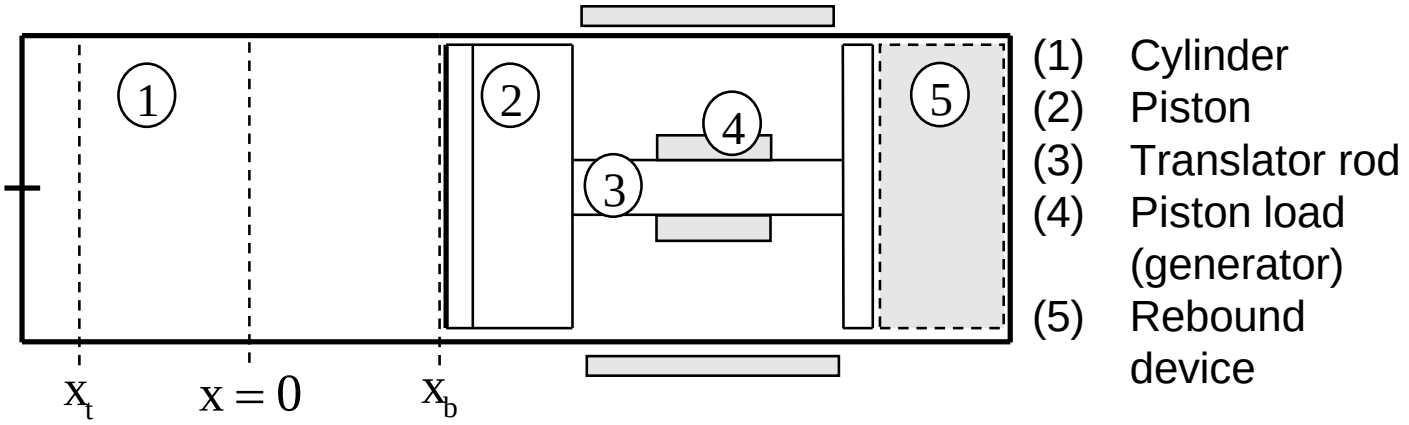

Figure 1. Generic FPE schematic. The piston, translator, and generator permanent magnet (for this illustration of an FPE generator) constitute the moving mass. The rebound device may be a mechanical spring, an air bounce chamber or another cylinder.

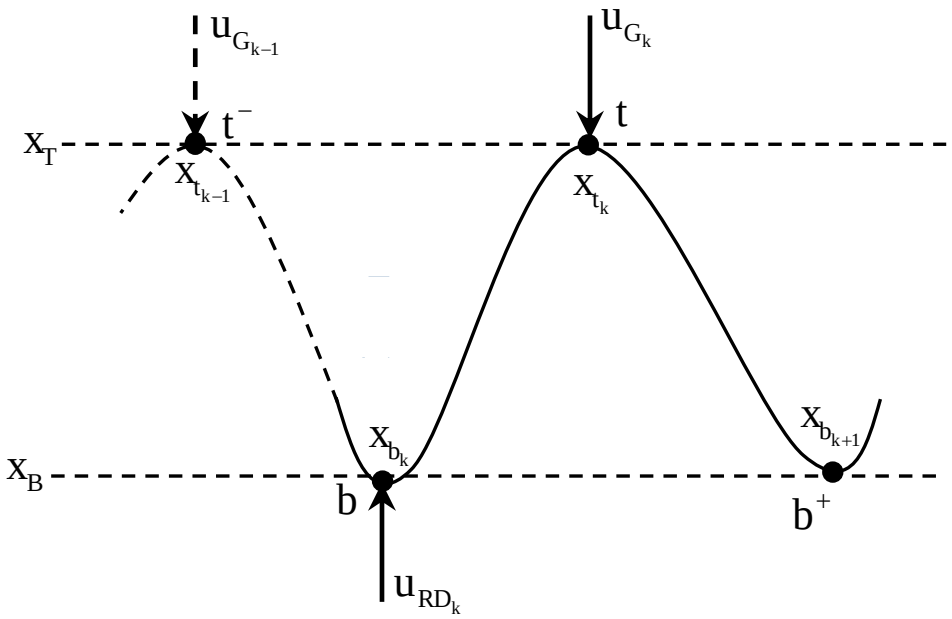

Figure 2. Visualization of piston motion over time annotated with notation used in analysis. One complete cycle is from b to b^+. The lines x_T and x_B are the nominal piston endpoints. The arrows represent inputs to the engine as fuel addition or rebound device stiffness adjustment.

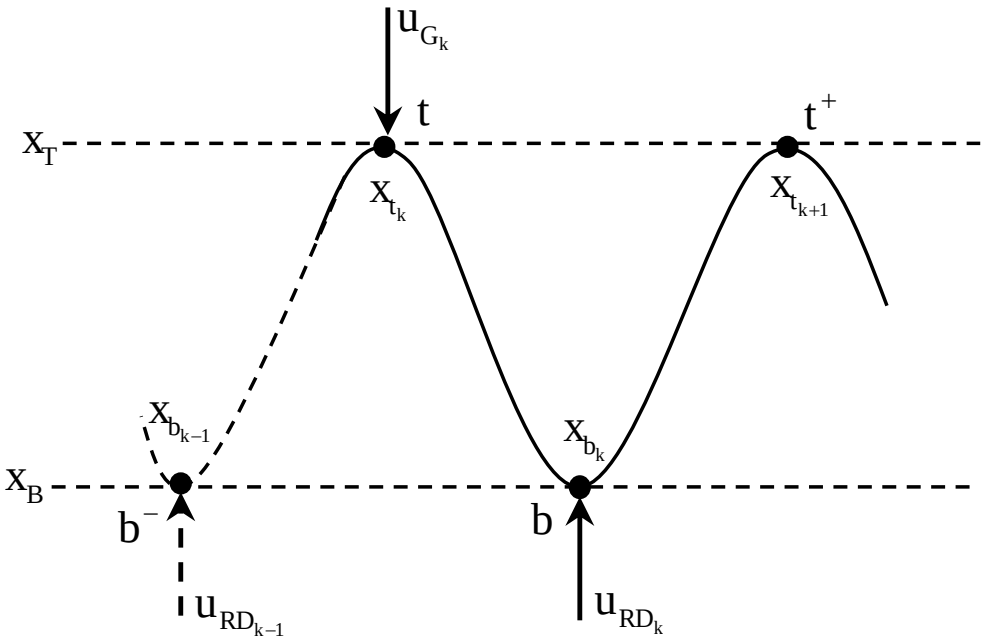

Figure 3. Visualization of piston motion over time annotated with notation used in analysis. One complete cycle is from t to t^+. The lines x_T and x_B are the nominal piston endpoints. The arrows represent inputs to the engine as fuel addition or rebound device stiffness adjustment.

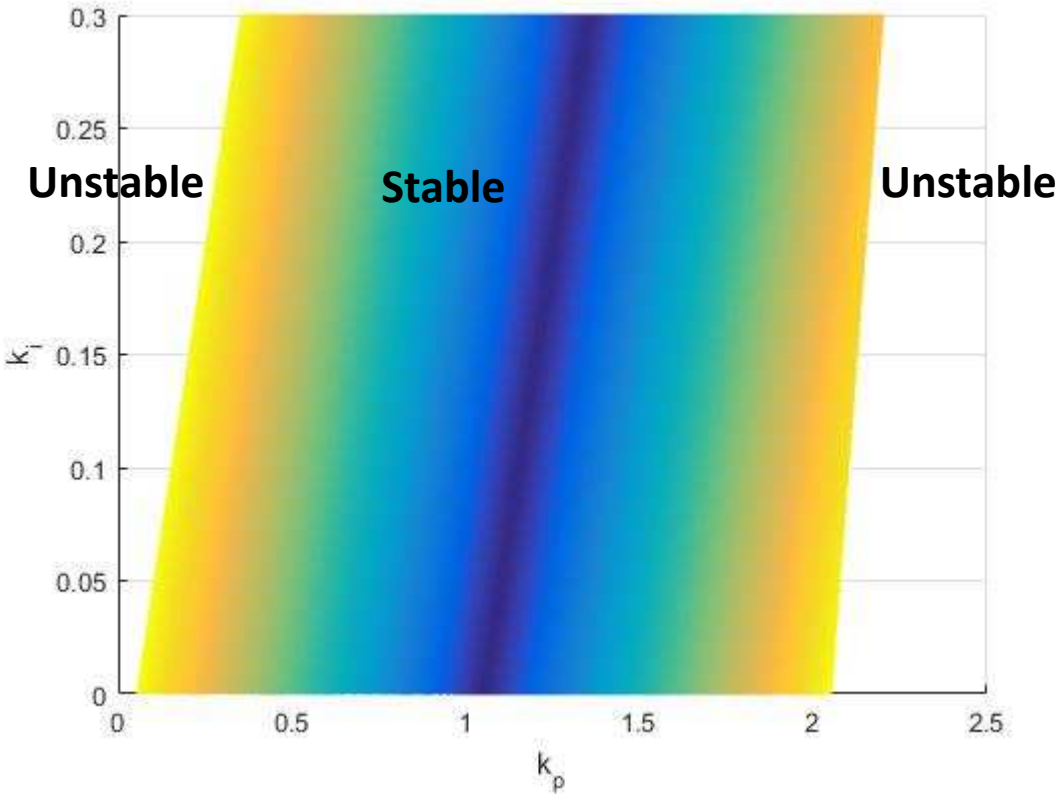

Figure 4. Parameter combinations k_p, k_i and associated regions of stability or instability, where $a = 1.05$ in system (24).

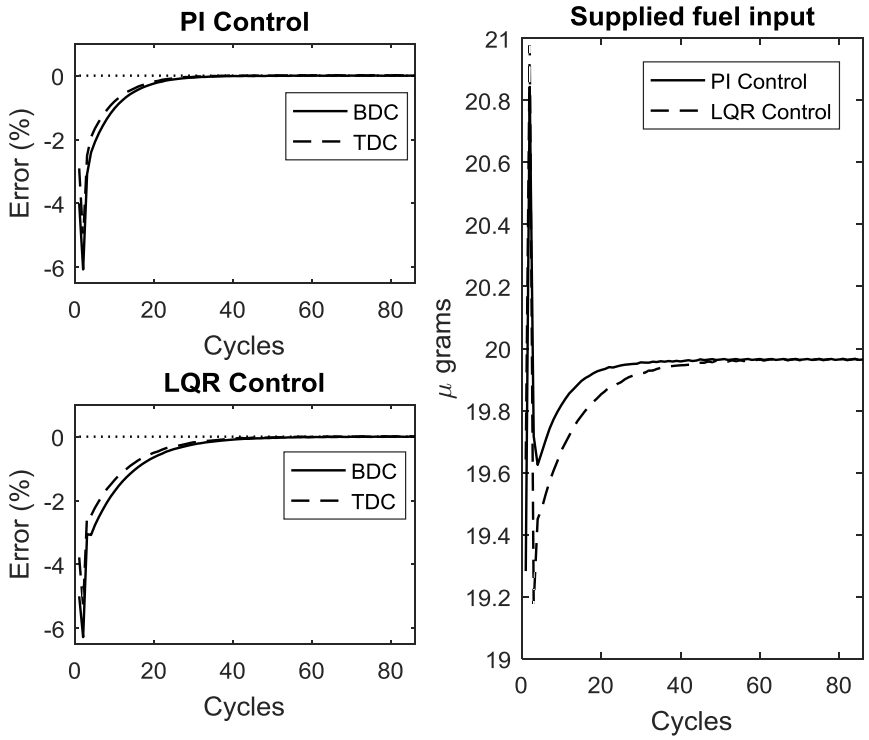

Figure 5. BDC/TDC error and input fuel response for PI and LQR controllers with a mechanical spring as rebound device. Controller parameters were chosen within their stability bounds. LQR response transient is slower than the PI response transient owing to a minimization of input objective.

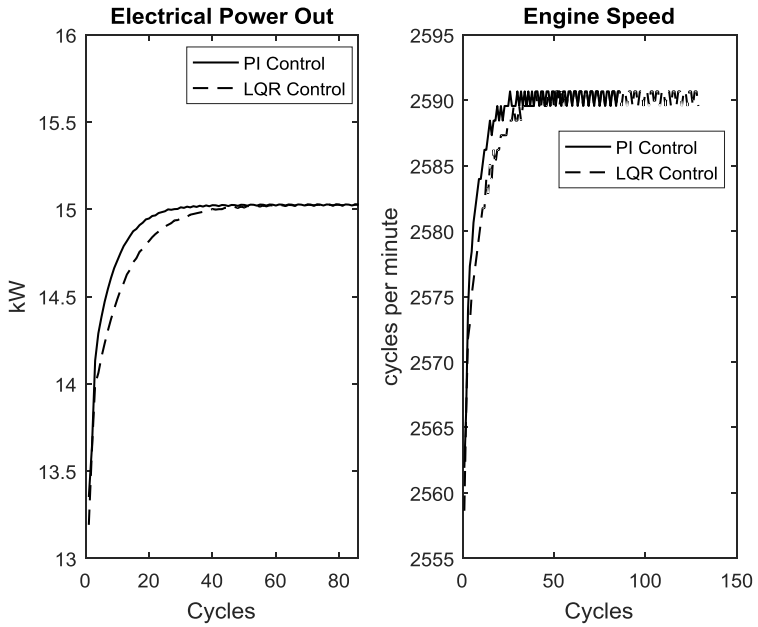

Figure 6. Output power and engine speed responses with a mechanical spring as rebound device. The same power and speed are achieved at steady state regardless of controller type.

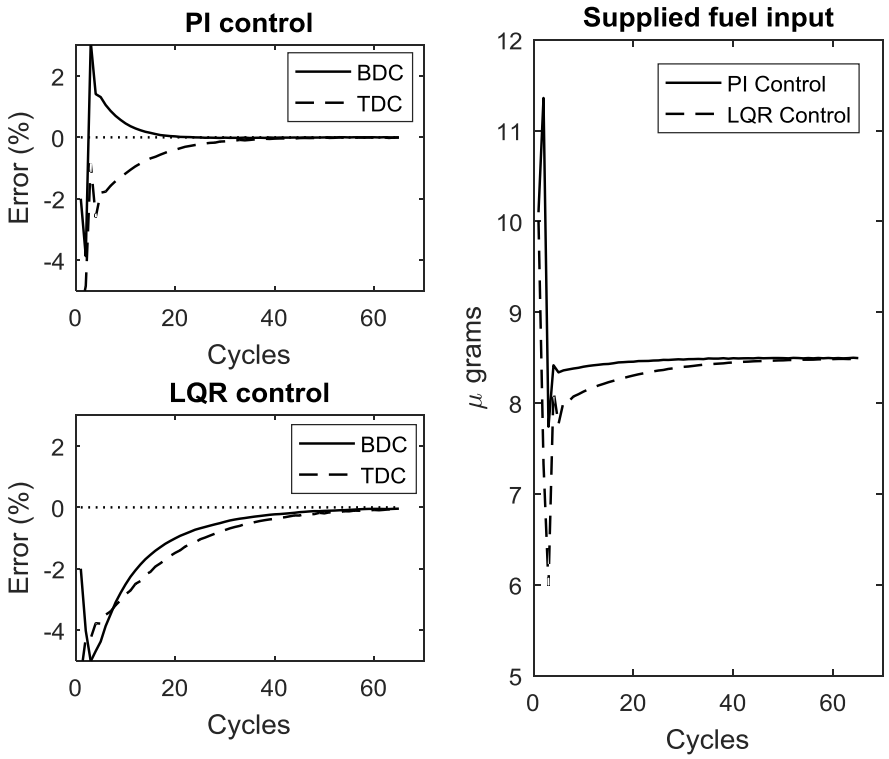

Figure 7. BDC/TDC error and input fuel response for PI and LQR controllers with a bounce chamber as rebound device. Controller parameters were chosen within their stability bounds. LQR response transient is slower than the PI response transient owing to a minimization of input objective.

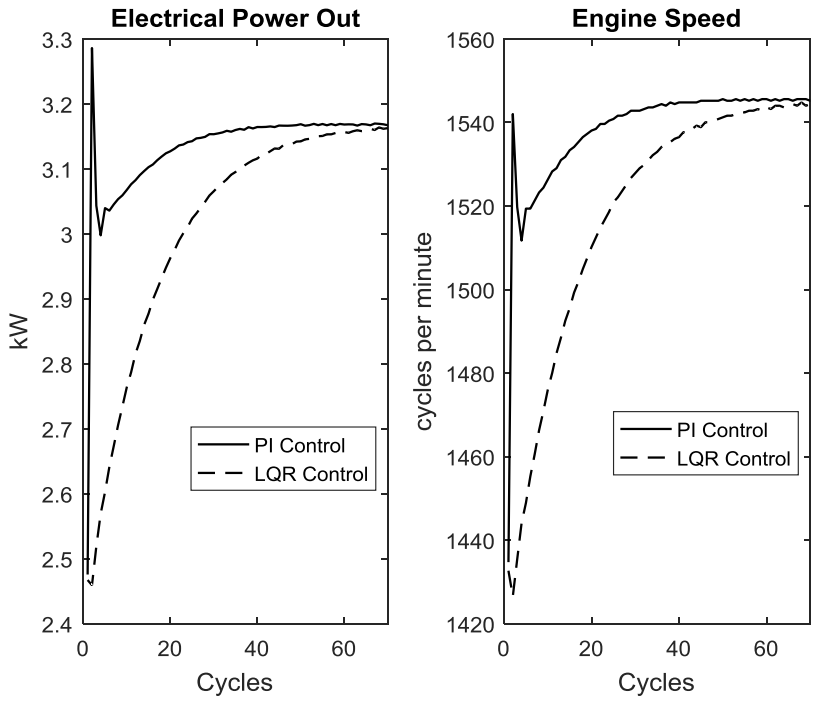

Figure 8. Output power and engine speed responses with a bounce chamber as rebound device. The same power and speed are achieved at steady state regardless of controller type.

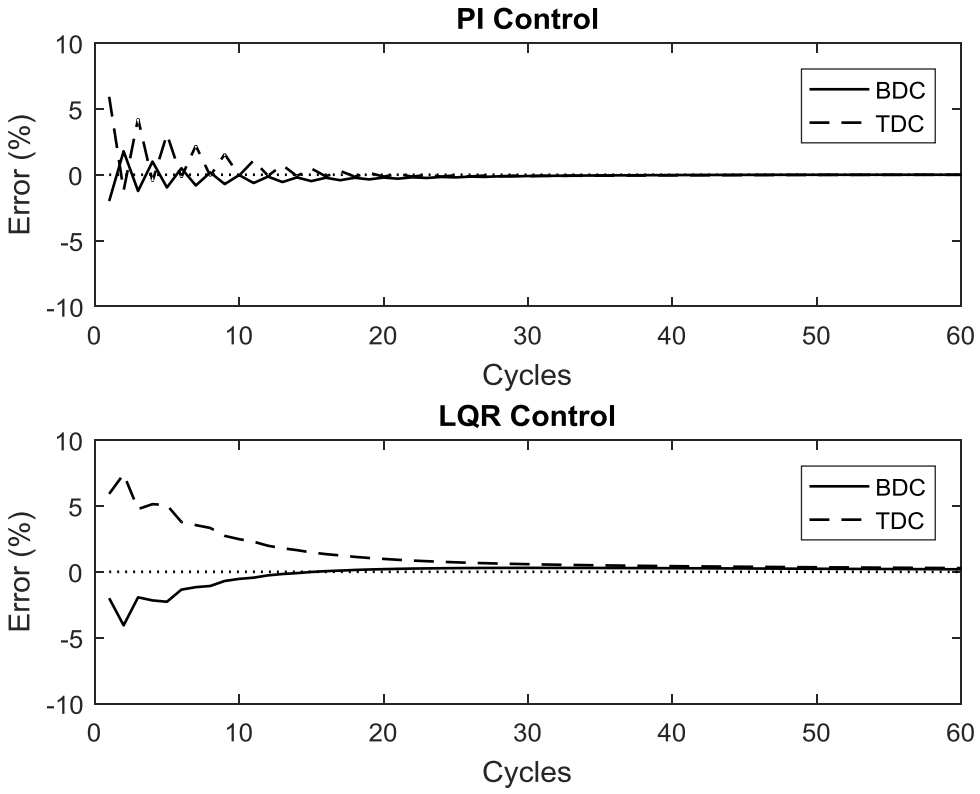

Figure 9. BDC/TDC error for PI and LQR controllers with a combustion chamber as rebound device. Controller parameters were chosen within their stability bounds. LQR response transient is slower than the PI response transient owing to a minimization of input objective.

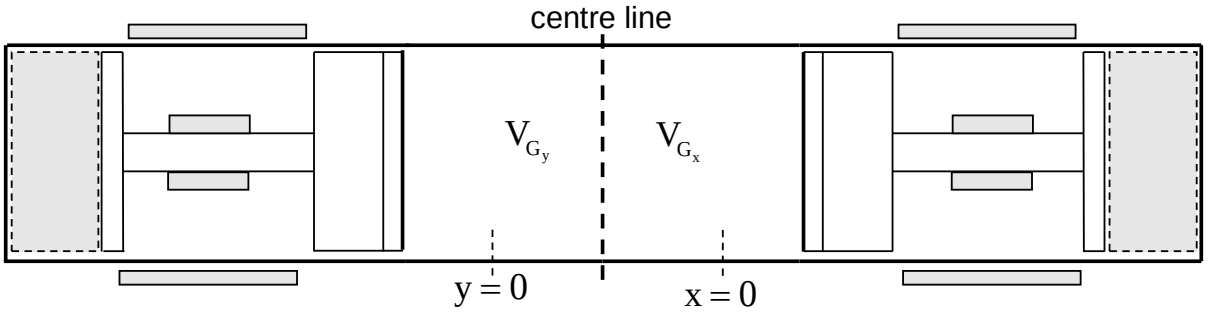

Figure 10. An opposed piston FPE. Two pistons sharing a combustion volume oppose each other about the centre line.